PAPER • **OPEN ACCESS**

Seismic responses of multi-story building isolated by Lead-Rubber Bearings considering effects of the vertical stiffness and buckling behaviors

To cite this article: Van-Tu Nguyen and Xuan-Dai Nguyen 2021 *IOP Conf. Ser.: Mater. Sci. Eng.* **1030** 012080

Seismic responses of multi-story building isolated by Lead-Rubber Bearings considering effects of the vertical stiffness and buckling behaviors

Van-Tu Nguyen and Xuan-Dai Nguyen

Institute of Techniques for Special Engineering, Le Quy Don Technical University, Viet Nam.

E-mail: nguyentu@lqdtu.edu.vn

Abstract. Elastomeric isolation bearing is one of the most commonly efficient devices and widely applied for protecting constructions in the earthquake regions. Its significant lateral deformation during operation, however, may affect its load-carrying capacity, especially the stability of the bearing. The current preliminary design method often focuses on shear behavior without effects of vertical stiffness and stability conditions that do not reflect the practical operation of devices. The paper presents the effect of vertical stiffness and buckling behavior on the seismic performance of lead-rubber bearing (LRB) used for seismic isolation in multi-story buildings. The effective parameters of LRB are estimated by the single-mode spectral analysis method, through a bilinear model, calculated by a typical target spectrum of Eurocode 8. A two-spring equivalent model is employed to study the effects of the vertical stiffness and critical buckling load that is varied as a function of lateral deformation. A set of time history nonlinear analysis is conducted to investigate the effects of vertical stiffness and critical buckling load on the seismic responses of building structures. The findings show the taking into account of the vertical stiffness and buckling behavior results in an increase of lateral displacements and a decrease of the lateral force and the floor acceleration of the isolated building.

1. Introduction

The multi-story building has been becoming popular and considered a feature of the infrastructure of big cities. However, its structure is sensitive to horizontal impacts, especially earthquakes. The conventional design method specified in many current codes [1–4], known as structural approaches, still has certain limitations such as low ductility ratio ($R \leq 5$), low capacity of energy dissipation. The accepted damages by this method might result in the interrupting operation and the requirement for repairs of structural construction after the earthquakes.

The advanced techniques for earthquake resistance, using seismic protection devices, are becoming more common for constructions in earthquake areas. These approaches allow a strengthening of the building structure by reducing the earthquake forces acting upon it. Their mechanisms are based on the higher dissipation energy capacity and/or higher value of available ductility that replaces the requirement for the original structures [5–10]. Among them, Seismic Base Isolation (SBI) has been considered an extremely efficient technique in minimizing the damage of building structure during seismic impacts. The main principle of SBI is introducing special supports with high vertical stiffness and significant lateral flexibility allowing the building structure to move more independently from the foundation under the ground motion [7–14]. In addition, the SBI provides a high capability of energy

dissipation, represented by an impressive damping ratio, which significantly reduces the displacement response and the force seismic transfer to the structure.

Based on the low horizontal stiffness, SBI increases significantly lateral displacements of the global structure. However, this lateral deformation occurs mostly in the bearing rather than the structural component of construction. The SBI, therefore, has often subjected to a large lateral deformation over its height during the operating. For the elastomeric bearing where its load-carrying capacity is strongly dependent on the compressive cross-section, this deformation may lead to a decrease in the horizontal stiffness and vertical stiffness of devices, reducing the performance of the device in both directions. In such conditions, it may lead to the collapse of devices or failure of construction with the two main failure modes commonly known as the tearing of the rubber and the buckling failure.

The effect of lateral deformation on the load-carrying capacity of isolators has been studied early and currently applied for the design of elastomeric bearing [7,8,15,16]. The obtained results have shown that the increase in the axial load and the lateral displacement leads to a decrease in the critical load and the horizontal stiffness of devices. Naeim and Kelly [8], presented the reduced area method to calculate the vertical stiffness where the reduction of the compressive cross-section during the operation of bearings is mentioned. Based on Haringx's works [17] to determine the stability of rubber rods, Gent [18] investigated the effect of axial load on the horizontal stiffness of elastomeric bearings, predicted the critical buckling load, and validated by experimental tests. To provide a visual physical model, the concept of the springs model is employed to investigate the mechanical properties of elastomeric bearing subjected to the combined axial force and horizontal deformation [19,20] that allow approximating the device behavior. Accordingly, the lateral stiffness and the vertical stiffness of the device are modeled by horizontal spring and rotational spring. The stiffness of springs is determined by the displacement caused by the respective load.

In the context of most current preliminary design approaches is often assumed that SBI has an impressive load-carrying capacity, these methods focus primarily on determining the horizontal stiffness and equivalent-damping ratio of SBI by an idealization bilinear model, without considering the horizontal-vertical coupling and buckling effects. It may result in inaccuracies for the actual operating of SBI, especially the elastomeric bearing. The evaluation of the final bearing properties subjected to the combined compression and lateral deformation is an essential part of the quantitative assessment, especially the stability of elastomeric bearing.

In this study, the effects of vertical stiffness and buckling behavior of LRB on the seismic response of the multi-story building are investigated. The theory of the two-spring model for the elastomeric bearing is first outlined to formulate the horizontal stiffness, the vertical stiffness, and the critical buckling load. The properties of bearings are firstly estimated by the simplified method through a single degree of freedom system using the specified design spectrum according to Eurocode 8. The design parameters are recalculated based on the device's structure for the analysis cases where the vertical stiffness and critical buckling load are mentioned. Finally, a set of five earthquake records are selected and calibrated to match the target spectrum to analyze nonlinear time history the seismic responses of a typical isolated building structure. The effects of vertical stiffness and the critical buckling load are investigated through the peak response of lateral force, displacement, and acceleration of the building structure.

2. Formulations for the vertical stiffness

2.1 Two-spring model

In this section, a mechanical model using two spring elements proposed by Koh and Kelly is considered to estimate the vertical stiffness of the elastomeric bearings subject to the lateral displacement [21] as shown in Figure 1. Accordingly, the model consists of a linear spring with horizontal stiffness, K_H, a rotational spring with stiffness, K_θ, two frictionless rollers, and a rigid tee supported by a pin with a total height, h.

The system is governed by a vertical loading P and a horizontal loading F, resulting in deformations such as a lateral displacement at the top of the column, Δ; a rotation about the pin, θ; a

vertical displacement, δv; and a deformation of the linear spring, *s*. Instead of the mechanical properties of an elastomeric seismic isolation bearing, its representation by an equivalent model's spring properties offers a simple physical understanding of the behavior under combined lateral and vertical loading [7].

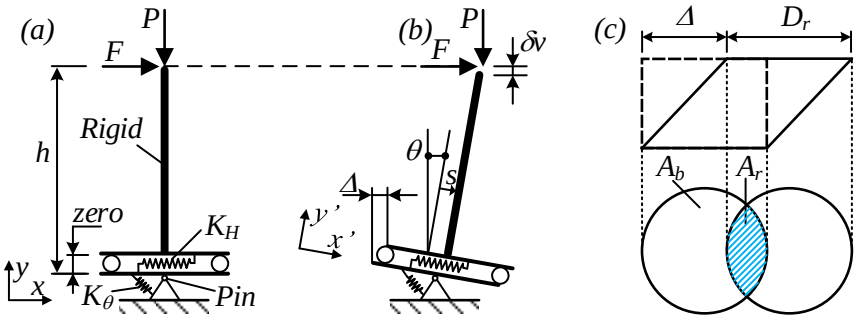

Figure 1. Two-spring model for elastomeric bearings and reduction in the bearing area: (a) underformed model, (b) deformed model, and (c) notation for reduced area of circular bearing.

As observation from Figure 1(a) and (b), the global deformation quantities Δ and δv, are related to the local deformation quantities of *s* and θ, through geometrical properties as the following Equations (1) and (2):

$$\Delta = s\cos\theta + h\sin\theta; \tag{1}$$

$$\delta_v = s\sin\theta + h\left(1-\cos\theta\right). \tag{2}$$

It is assumed that the angle of rotation is small enough, therefore: $sin\theta \approx \theta$, $cos\theta \approx 1$, $1 - cos\theta = 2sin^2(\theta/2) \approx \theta^2/2$.

Further, the equilibrium equations are obtained from the deformed configuration of the model is expressed as the following:

$$\sum F_{x'}: \quad -P\theta + K_H s = F; \tag{3}$$

$$\sum M_{pin}: \quad \left(K_\theta - Ph\right)\theta - Ps = Fh. \tag{4}$$

Considering the case of $K_\theta \to \infty$, the deformation is determined as a function of K_H, which is equal to the shear stiffness of an elastomeric bearing. On the other hand, when $K_H \to \infty$, the stiffness of the rotational spring K_θ is related to the Euler buckling load and $F = 0$ (no shear deformations). Accordingly, the obtained spring properties as:

$$K_{H0} = G_r A_s / h;\ K_\theta = P_E h, \tag{5}$$

where: G_r is the shear modulus of rubber; $A_s = A_b h / h_r$; A_b is the bonded rubber area; $P_E = \pi^2 E I_s / h^2$, $I_s = I \times h / h_r$; *I* is the moment inertia of the cross-section; *E* is the modulus of elasticity, $E = E_c / 3$. Accordingly, the vertical displacement is obtained as the following equation:

$$\delta_v = \frac{\Delta^2}{2h} \times \frac{\left(G_r A_s + P\right)\left(P + G_r A_s + 2P_E\right)}{\left(G_r A_s + P + P_E\right)^2}. \tag{6}$$

For seismic isolation bearings, it is reasonable to assume $G_r A_s \gg P_E$ and $P \gg P_E$, by neglecting the $G_r A_s$ and *P* terms where they are summed with P_E.

Finally, the total vertical displacement, including the deformation caused by the applied compressive load and the lateral displacements is obtained as the following:

$$\delta_{vt} = \frac{P}{K_{vo}} + \frac{3\left(G_r A_b h + P h_r\right)\Delta^2}{\pi^2 E_c I}, \tag{7}$$

where $K_{v0} = E_c A_b / h_r$ is the initial vertical stiffness of the bearing (without lateral displacement); and E_c is the instantaneous compression modulus of the rubber-steel composite that is controlled by the shape factor, S - the ratios of the loaded area of rubber layer and the surrounding area on the side of a single rubber layer.

With a circular pad of diameter D_r and a single rubber layer thickness t_r as shown in Figure 2:

$$E_c = 6G_r S^2; S = D_r / 4t_r. \tag{8}$$

The vertical stiffness is obtained by inverting the result of (7) with respect to the vertical load, P. The vertical stiffness of the bearing is determined as:

$$K_v = K_{v0}\left(1 + \frac{3A_b}{I} \times \frac{\Delta^2}{\pi^2}\right)^{-1}. \tag{9}$$

2.2 Reduced area of bearing

Generally, the compressive cross-section of isolators is considerably reduced by the lateral deformation during operation, resulting in a significant decrease in the vertical stiffness as the presented results of Buckle and Liu [22]. This concept is based on a model of a column with a reduced area [7,16], as shown in Figure 1(c). Accordingly, for the LBR subjects to a shear displacement, Δ, the critical buckling load is decrease and give by the following expression:

$$P_{crre} = P_{cr} \times \left(A_r / A_b\right), \tag{10}$$

where P_{crre} is the buckling load at the reduced area, P_{cr} is the buckling load at zero displacement [21]

$$P_{cr} = \sqrt{P_E G_r A_s}. \tag{11}$$

For circular bearings of bounded area of diameter D_r, the reduced area A_r is calculated as:

$$A_r = \frac{D_r^2}{2}\left[\cos^{-1}\left(\frac{\Delta}{D_r}\right) - \frac{\Delta\sqrt{D_r^2 - \Delta^2}}{D_r^2}\right]. \tag{12}$$

As an observation from Equation (10), the bearing may present zero capacity when the acted horizontal displacement equal to the diameter of the bearing. However, the LBR will not lose total stability when the overlapping area is equal to zero, as observed from the experimental tests [19,23,24]. Therefore, an appropriate function of the reduced critical buckling load of LRB should be taken into account, as proposed formula by Warn et al. [19]:

$$P_{crre} = \begin{cases} P_{cr} \times \left(A_r / A_b\right) & A_r / A_b \geq 0.2; \\ 0.2 P_{cr} & A_r / A_b < 0.2. \end{cases} \tag{13}$$

The vertical stiffness with accounting for the reduced area is determined as the follows:

$$K_v = K_{v0} \times \left(A_r / A_b\right). \tag{14}$$

3. Equivalent bilinear model of lead-rubber bearing

Lead-rubber bearing consists of an elastomeric bearing with a central core of lead, shown in Figure 2. Its geometric properties include the lead diameter (d_L), bearing's total diameter (D_r), steel shim thickness (t_s), single rubber layer thickness (t_r), number of rubber layers (n_r), rubber's total thickness (h_r=n_rxh_r), bearing's total height (rubber and steel shim) (h) and the total height of bearing included connecting plate (H). Practically, LRB devices provide a great equivalent damping ratio (up to 30%) and also be easily modified by the change of the appropriate size of the lead plug [1,3,8].

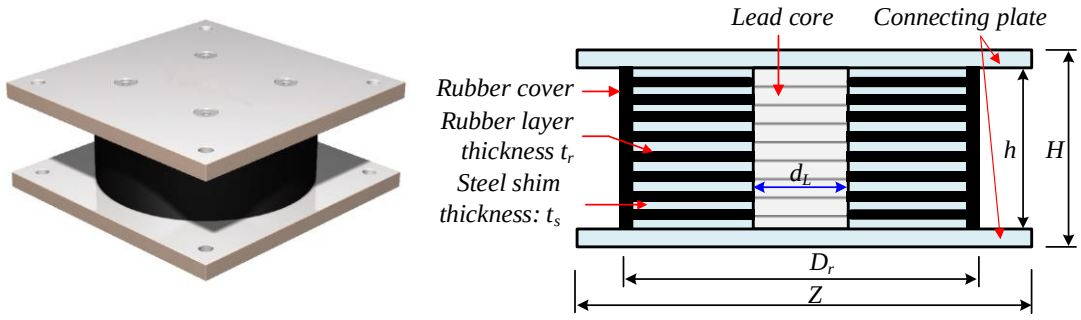

Figure 2. Details for lead-rubber bearing.

3.1 Horizontal stiffness of devices without accounting for axial load

In practical, SBI is often modeled by a bilinear model with four main parameters such as the characteristic strength, Q; the post-yielding stiffness, K_2; the yield displacement, D_y; and the maximum displacement, D_{max}, as shown in Figure 3 [8].

The effective stiffness, K_{eff}, of equivalent model can be determined as follows:

$$K_{eff} = F_{\max}/D_{\max} = MS_a\left(T_{eff},\xi_{eff}\right)/D_{\max}, \tag{15}$$

where

M is the mass total of construction on the LBR (ton);

T_{eff} is the effective period of the isolation system (sec);

$S_a(T)$ is the elastic response acceleration spectrum;

ξ_{eff} is the effective equivalent viscous damping ratio, expressed as a percentage.

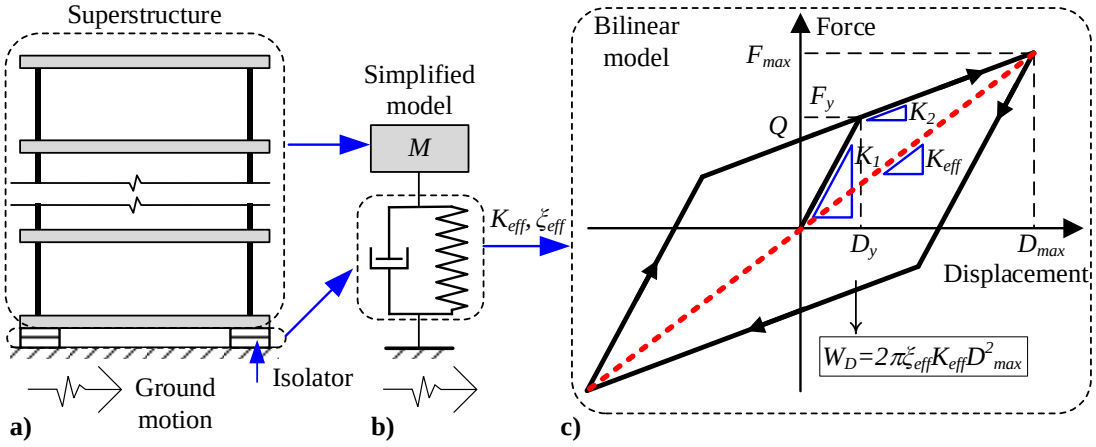

Figure 3. Simplified model of isolated building and equivalent bilinear model of isolator.

The energy dissipated per cycle (EDC) is determined by the area under the hysteresis loop and considered by an equivalent linear viscoelastic system, therefore:

$$\xi_{eff} = \frac{EDC}{2\pi K_{eff} D_{\max}^2} = \frac{4Q\left(D_{\max} - D_y\right)}{2\pi K_{eff} D_{\max}^2}. \tag{16}$$

The two stiffness of bilinear model (K_1, K_2) are determined as follows:

$$K_1 = Q/D_y + K_2; K_2 = K_{eff} - Q/D_{\max}. \tag{17}$$

Because these equations are coupled with each other, it is necessary to use an iterative procedure to calculate the design parameters. To do so, a calculation program SBI properties based on Matlab software is conducted (SBIP program).

On focus to the application of LRB, it should be noted that the contribution of rubber component is significantly to the stiffness of bearing, meanwhile, its effects on the characteristic strength of the device (Q) (including the yield force, F_y) are relatively negligible when compared with the lead plug. Therefore, Q and F_y can be approximated only by the lead core as follows:

$$F_y = \frac{1}{\psi} f_{yL} \frac{\pi d_L^2}{4}; Q = F_y(1-\alpha), \tag{18}$$

where f_{yL} is the shear yield stress of lead, d_L is the diameter of the lead plug ($D_r / 6 < d_L < D_r / 3$) [25], ψ is load factor accounting for creep in lead (ψ =1 for seismic loads), and $\alpha = K_2/K_1$ is the post-elastic ratio, taken in the range of α =[1/30÷1/15] for the lead-plug rubber bearing [8].

3.2 Horizontal stiffness of devices with accounting for axial load

When the load carried by the LBR is comparable to the critical buckling load, the horizontal stiffness K_H is determined as the following [8]

$$K_H = \frac{G_r A_s}{h} \times \left[1 - \left(\frac{P}{P_{cr}}\right)^2\right] = K_{H0} \times \left[1 - \left(\frac{P}{P_{cr}}\right)^2\right]. \tag{19}$$

4. Numerical analysis

4.1 Description of the building structure

In order to investigate the seismic nonlinear time history response, a set of numerical analysis for a typical isolated building structure is performed. The selected building structure characterizes the resident buildings in cities where the impact of earthquakes is significant. In addition, the fundamental vibration mode of structure (1.3 s for fixed-base model and 3.0 s for isolated-base model) allows a clear demonstration of the efficiency of SBI. Accordingly, a model 3D of the selected multi-story building is detailed as below:

- The reinforced concrete building has 15 floors. The floor height is 3.9 m for the stories and 3.6 m for the basement. The plan has three bays in the X, Y direction, as shown in Figure 4 (a).
- Structural component includes: the cross-section of main beam systems is 35cm x 75cm (width x depth), the cross-section of sub-beam is 30cm x 60 cm, the cross-section of foundation beam is 80cm x100cm. The cross-section dimensions of columns: from 1st to 6th story 100cm x 100cm; from 7th to 11th story 90cm x 90cm; from 12th to the roof 80cm x 80cm. The concrete wall thickness is 35cm; and the floor thickness is 15cm, and the basement floor is 20cm.
- Grade of structural concrete: C35/45 (EN 1993-1-1).
- Load acting: the floor loading: dead load 100 daN/m2, live load 200 daN/m2 and the roof loading: dead load 150 daN/m2, live load 100 daN/m2 .

The designed building is supported on the soil type C and located in the region with the design ground acceleration according to Eurocode 8 [4], representative by with a_{gR} = 0.25g. Early studies have been found no major difference in quantities of seismic response obtained from the nonlinear time history analyses using the records scaled to match the elastic design spectra and the response spectra [26–28], especially for long periods like isolated structure responses. Therefore, earthquake records are scaled to match the target spectrum determined by EC8 with 5% damping to uniformly the design procedure (spectral analysis - simplified method and nonlinear time- history analysis method). To do so, a suite of five historic ground motions (larger than the requirement of EC8 – at least 3 records) is selected as shown in Table 1. These ground motions are selected with various magnitudes, epicenter distances, and peak ground accelerations ensuring the randomness and diversity of earthquake waves.

The spectra of scaled records are performed in Figure 5. A slight difference between the spectrum of each ground motion and the target spectrum is found, especially for the short periods. However, the mean spectrum is found in an excellent match with the design spectra, as shown in Figure 5.

Table 1. Earthquake records selected for analyses [29].

#	Earthquake, station	Nation, date	Mw	R (km)	PGA (g)
Acc1	Saguenay, Chicoutimi-Nord	Canada, 25-11-1988	5.9	43	0.131
Acc2	Chi-Chi, Taichung	Taiwan, 25-9-1999	6.3	10	0.774
Acc3	Loma Prieta, San Francisco	US, 17-9-1989	7.0	98	0.199
Acc4	Nahanni, Bettlement Creek-S3	Canada, 23-12- 1985	6.5	24	0.194
Acc5	Northridge, Castaic-Old Ridge Rte	US, 17-01-1994	6.7	41	0.568

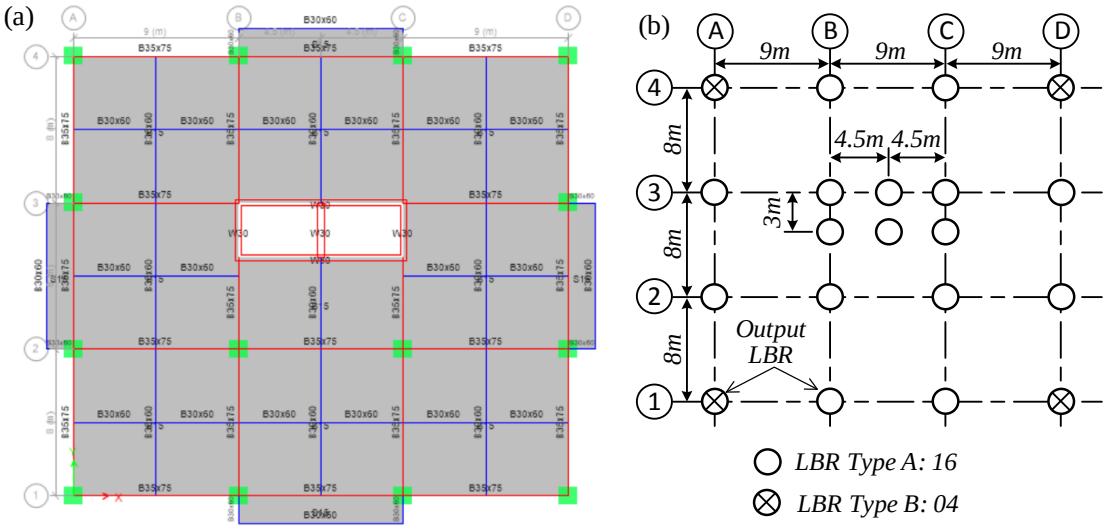

Figure 4. Specific floor plan model of the building analyzed (a) and LBR plan for designed (b).

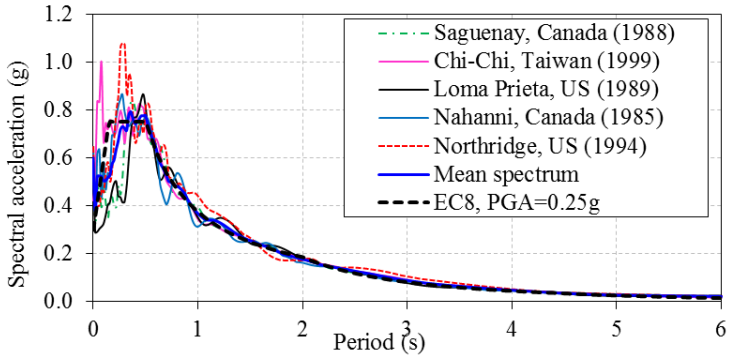

Figure 5. Ground motion time history and spectral acceleration used for study.

4.2 Design the LRB as seismic isolation systems for building

In the numerical model using Etabs software [30], the seismic isolators are modeled by nonlinear link elements instead of the fixed-base constraint in the conventional structure. According to the structural plan of building, 20 single bearing isolators (SBI) include 16 SBI type A and 4 SBI type B is used for isolate the considered building structure as shown in Figure 4(b).

The maximum mass acts on the SBIs is determined such as M =726 (ton) for one SBI type A and M =380 (ton) for one SBI type B that use to estimate the parameters of isolators. Assume that the equivalent damping ratio of isolator is ξ_{eff} = 20% (according to LRB); the effective period of the fundamental mode of isolated building is assumed, T_{eff} =2.5 *s*, the post-elastic ratio α = 1/21 for LRB [8].

Based on SBIP program, the estimated properties of two types of SBI are detailed in Table 2. Correspondingly, based on standard EN 1337-3 2005 [3], the selected circular and designed parameters of each SBI type are shown in Table 3.

Table 2. The required properties of 2 SBI types.

SBI	M (ton)	K_{eff} (kN/m)	K_1 (kN/m)	K_2 (kN/m)	Q (kN)	D_{max} (mm)	D_y (mm)
Type A	726	4586	65312	3110	200	135.55	3.22
Type B	380	2400	34188	1628	105	135.55	3.22

Table 3. Geometrical properties of SBIs considered.

SBI	D_r (mm)	d_L (mm)	h_r (mm)	h (mm)	H (mm)
Type A	800	200	112 (7x16)	142 (112+6x5)	206 (142+2x32)
Type B	650	150	120 (10x12)	156 (120+9x4)	206 (156+2x25)

The material parameters of rubber and lead are selected as G_r=0.9 MPa and f_{yL}=9 MPa. Based on the dimensions of SBIs in Table 3, the parameters for SBI, representative by the link elements in Etabs software, with four considered analysis cases are recalculated. The obtained results are shown in Table 4.

Table 4. Design parameters of SBI for numerical model.

SBI	K_{eff}(kN/m)	C_{eff}(kNs/m)	K_1(kN/m)	K_2(kN/m)	Q(kN)	K_v(kN/m)	C_v(kNs/m)
Case 1: Only horizontal stiffness of SBI is considered							
Type A	3787	1081	37804	1800	269	∞	∞
Type B	2356	558	26014	1239	151	∞	∞
Case 2: Horizontal stiffness and vertical stiffness of SBI are considered							
Type A	3787	1081	37804	1800	269	2973738	4646
Type B	2356	558	26014	1239	151	2016499	2768
Case 3: Horizontal stiffness and buckling behavior of SBI are considered							
Type A	3415	1139	29998	1428	269	∞	∞
Type B	2107	815	20772	989	151	∞	∞
Case 4: Horizontal stiffness, vertical stiffness and buckling behavior of SBI are considered							
Type A	3415	1139	29998	1428	269	2973738	4646
Type B	2107	815	20772	989	151	2016499	2768

4.3 Results and discussions

The hysteresis response of isolators is illustrated in Figure 6 for two specific isolators (type A and type B), corresponding to axis 1-A and 1-B, respectively. Practically, the drift of building structures occurs mainly at the isolators' level, corresponding to the fundamental modal of vibration. The same devices logically produce the same hysteresis response. In such contexts, the seismic response of the isolator at axis 1-A (type A) is selected as a typical location to investigate the effects of the vertical stiffness and critical buckling behaviors on its seismic response.

Figure 6(b) shows the hysteresis response of the isolator type A, corresponding to the four considered analysis cases with Saguenay (Canada, 25-11-1988) earthquake record. As observations from the figures, the effect of vertical stiffness and buckling behavior generally leads to an increase in the displacement maximum, logically resulting in a reduction of lateral forces and floor accelerations.

The value of D_{max} is minimum for the model considering only horizontal stiffness of SBI (case 1, corresponding to the existing preliminary design approaches of SBI), and D_{max} is maximum when horizontal stiffness, vertical stiffness, and critical buckling load are considered (case 4 that is more suitable for the actual operating of SBI). The time history responses of the shear force and the lateral displacement for these two cases shown in Figure 7(a) and (b), respectively.

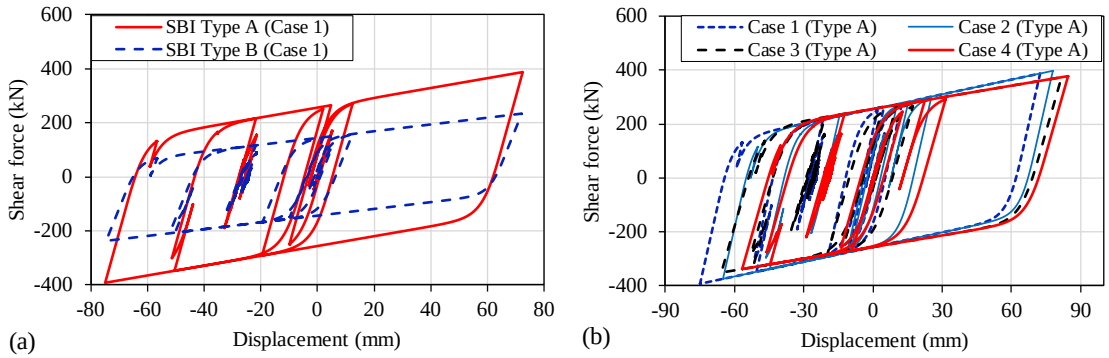

Figure 6. Hysteresis responses of isolators: (a) two typical isolators and (b) isolators type A for four analysis cases with Saguenay (Canada, 25-11-1988) earthquake record.

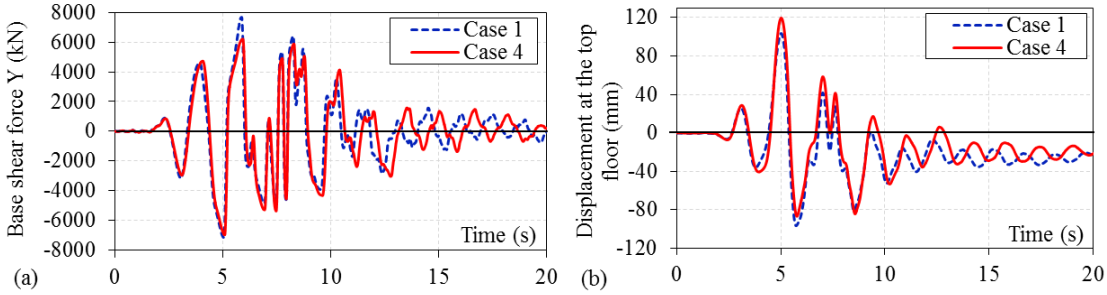

Figure 7. Time history responses: (a) base shear forces and (b) and lateral displacements with Saguenay (Canada, 25-11-1988) earthquake record.

Figure 8 and Table 5 show the comparisons of peak responses in the displacement, the base shear force, and the top floor acceleration of five ground motions. Similar tendencies of seismic responses of the component accelerations as well as the mean response are obtained.

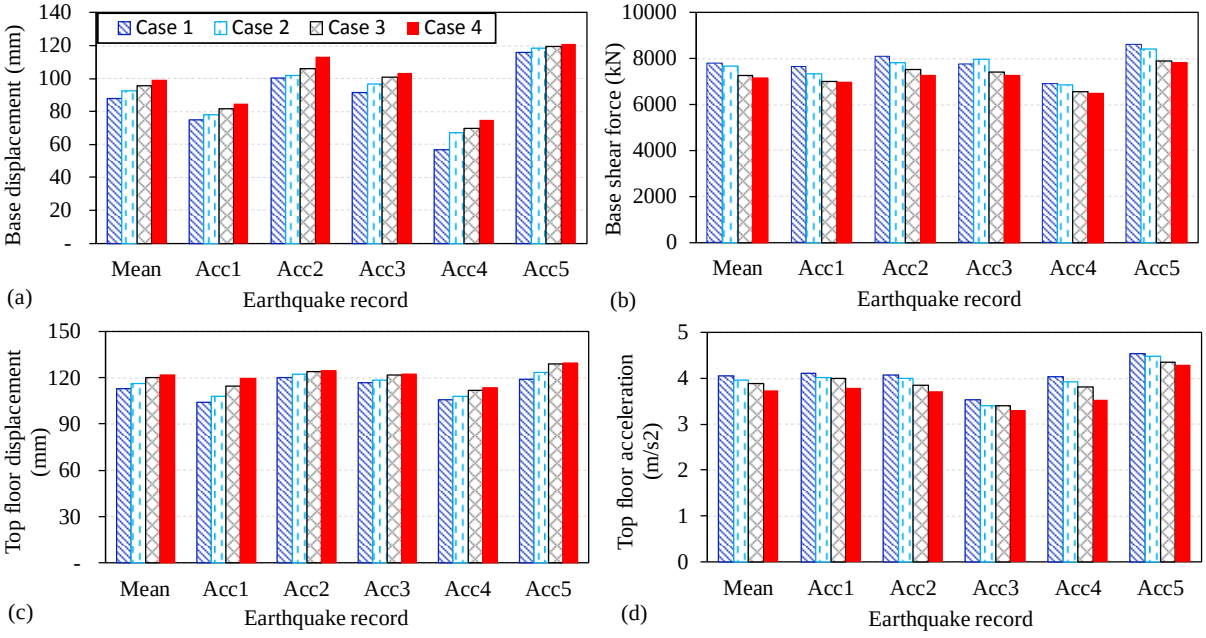

Figure 8. Comparison of peak seismic responses: (a) base displacement, (b) base shear forces, (c) top floor displacement, and (d) top floor acceleration with earthquake records.

Table 5. Comparisons of mean seismic responses between cases analyzed.

Mean seismic response	Case 1	Case 2	Case 3	Case 4	Compare C4 and C1 (%)
Base displacement (mm)	87.89	92.51	95.65	99.50	13.2
Base shear force (kN)	7805	7669	7281	7164	-8.2
Top floor displacement (mm)	113.05	115.91	120.16	121.76	7.7
Top floor Acceleration (m/s^2)	4.06	3.97	3.89	3.74	-7.9

It shows that taking into account vertical stiffness and critical buckling load leads to an increase in the maximum displacement and a decrease in the shear force and the floor acceleration. These changes, around 10%, seem to be insignificant. The increase in the lateral displacement, however, is of interest, especially in the context that this displacement occurs mainly at the seismic bearing in the isolated building structure that may affect the displacement capacity of devices.

5. Conclusions

In this paper, a numerical study of the effect of the vertical stiffness and the critical buckling load of Lead-Rubber Bearing on the seismic responses of isolated buildings is presented. The properties of bearings are firstly estimated by the simplified method with only horizontal stiffness mentioned. The vertical stiffness and the critical buckling load then determined based on the selected size of devices. Time history nonlinear analyses are performed on 3D models of a typical multi-story building to investigate the variation of seismic responses, by using five earthquake records calibrated to match the target spectrum of Eurocode 8. The following conclusions are summarized:

- The considering of the vertical stiffness and the critical buckling load leads to a decrease in the horizontal stiffness of bearings. Whereby, the peak response of base shear force and the top floor acceleration decrease, and the maximum displacement increases.
- Although existing preliminary design approaches provide conservative estimates for the lateral force. However, the effects of the vertical stiffness and the critical buckling load should be taken into account in the selecting and sizing of the devices to ensure the displacement capacity and the stability of bearings during the operation.

References

[1] AASHTO 2014 *Guide Specifications for Seismic Isolation Design* (Washington, DC.) p 463
[2] ASCE/SEI 7-10 2010 *Minimum Design Loads for Buildings and Other Structures* (Reston, VA)
[3] EN 1337-3 2005 *Structural Bearings - Part 3: Elastomeric bearings* (Brussels: CEN) p 94
[4] EN 1998-1 Eurocode 8 2005 *Design of Structures for Earthquake Resistance. Part 1: General Rules, Seismic Actions and Rules for Buildings* (London: CEN) p 229
[5] Cheng F Y, Jiang H and Lou K 2008 *Smart Structures: Innovative Systems for Seismic Response Control* (USA: CRC Press) p 643
[6] Aiqun Li 2020 *Vibration Control for Building Structures: Theory and Application* (Switzerland: Springer) p 677
[7] Kelly J M 1993 *Earthquake-Resistant Design with Rubber* (London: Springer-Verlag) p 134
[8] Naeim F and Kelly J M 1999 *Design of Seismic Isolated Structures: From Theory to Practice* (Canada: John Wiley & Sons, INC) p 289
[9] Sahu G and Sahu P 2019 Comparative analysis of effects of base isolator & fluid viscous damper on response of a RCC structure *IRJET* **6** 94–101
[10] Shevale S S, Kadam S S, Pise C P, Pawar Y P, Deshmukh C M and Mohite D D 2016 Seismic behaviour of multi-storied building by using tuned mass damper and base isolation : A Review *J. of Eng. Res. and Appl.* **6** 1–6
[11] Chopra A K 2017 *Dynamics of structures. Theory and applications to earthquake engineering* (Boston: Prentice Hall) p 980

[12] Warn G P and Ryan K L 2012 A review of seismic isolation for buildings: Historical development and research needs *Buildings* **2** 300–25
[13] Makris N 2019 Seismic isolation: Early history *Earth. Eng. & Struct. Dyn.* **48** 269–83
[14] Nath S, Debnath N and Choudhury S 2018 Methods for improving the seismic performance of structures - A review *IOP Conf. Series: Mat. Sci. and Eng.* **377**
[15] Nagarajaiah S and Ferrell K 1999 Stability of elastomeric seismic isolation bearings *J. of Struct. Eng.* **125** 946–54
[16] Buckle I G, Itani A and Monzon E 2017 Stability of elastomeric isolation systems *NZSEE Conf.* pp 0–7
[17] Haringx JA 1948 On highly compressible helical springs and rubber rods, and their application for vibration-free mountings *Philips Research Reports* **4** 49–80
[18] Gent B A N 1964 Elastic stability of rubber compression springs *J. Mech. Eng. Sci.* **6** 318–26
[19] Warn G P, Whittaker A S and Constantinou M C 2007 Vertical stiffness of elastomeric and lead – rubber seismic isolation bearings *J. of Struct. Eng.* **133** 1227–36
[20] Koh C G and Kelly J M 1987 *Effects of Axial Load on Elastomeric Isolation Bearings* (University of California, Berkeley, CA: Earthquake Engineering Research Center)
[21] Koh C G and Kelly J M 1988 A simple mechanical model for elastomeric bearings used in base isolation *Int. J. Mech. Sci.* **30** 933–43
[22] Buckle I G and Liu H. 1993 Stability of elastomeric seismic isolation systems *Proc. of the SSIPEDC* (Redwood City, California) pp 293–305
[23] Sanchez J, Masroor A, Mosqueda G and Ryan K 2013 Static and dynamic stability of elastomeric bearings for seismic protection of structures *J. of Struct. Eng.* **139** 1149–59
[24] Weisman J and Warn G P 2012 Stability of elastomeric and lead-rubber seismic isolation bearings *J. of Struct. Eng.* **138** 215–23
[25] Buckle I G, Constantinou M C, Dicleli M and Ghasemi H 2006 *Seismic Isolation of Highway Bridges* (MCEER, University at Buffalo, the State University of New York)
[26] Ucar T and Merter O 2019 Effect of design spectral shape on inelastic response of RC frames subjected to spectrum matched ground motions *Struct. Eng. and Mech.* **69** 293–306
[27] Samanta A and Pandey P 2018 Effects of ground motion modification methods and ground motion duration on seismic performance of a 15-storied building *J. of Build. Eng.* **15** 14–25
[28] Pant D R and Maharjan M 2016 On selection and scaling of ground motions for analysis of seismically isolated structures *Earth. Eng. and Eng. Vibrat.* **15** 633–48
[29] CESMD 2020 The Center for Engineering Strong-Motion Data
[30] CSI 2018 Etabs Version 17.0.1.